J|A|C|S ARTICLES

Published on Web 05/24/2010

Nanoscale Morphology in Precisely Sequenced Poly(ethylene-*co*-acrylic acid) Zinc Ionomers

Michelle E. Seitz,[†] Christopher D. Chan,[‡,§] Kathleen L. Opper,[⊥] Travis W. Baughman,[⊥,¶] Kenneth B. Wagener,[⊥] and Karen I. Winey*[,†,‡]

Department of Materials Science and Engineering, University of Pennsylvania, Philadelphia, Pennsylvania 19104, Department of Chemical and Biomolecular Engineering, University of Pennsylvania, Philadelphia, Pennsylvania 19104, and Department of Chemistry, University of Florida, Gainesville, Florida 32611

Received March 17, 2010; E-mail: winey@seas.upenn.edu

Abstract: The morphology of a series of linear poly(ethylene-*co*-acrylic acid) zinc-neutralized ionomers with either precisely or randomly spaced acid groups was investigated using X-ray scattering, differential scanning calorimetry (DSC), and scanning transmission electron microscopy (STEM). Scattering from semicrystalline, precise ionomers has contributions from acid layers associated with the crystallites and ionic aggregates dispersed in the amorphous phase. The precisely controlled acid spacing in these ionomers reduces the polydispersity in the aggregate correlation length and yields more intense, well-defined scattering peaks. Remarkably, the ionic aggregates in an amorphous, precise ionomer with 22 mol % acid and 66% neutralization adopt a cubic lattice; this is the first report of ionic aggregate self-assembly onto a lattice in an ionomer with an all-carbon backbone. Aggregate size is insensitive to acid content or neutralization level. As the acid content increases from 9.5 to 22 mol % at ~75% neutralization, the number density of aggregates increases by ~5 times, suggesting that the ionic aggregates become less ionic with increasing acid content.

Introduction

Ionomers are polymers with a relatively small fraction of ionic groups covalently bonded to the backbone as pendant moieties[1] and have tremendous commercial utility because of property enhancements caused by microphase separation of the nonpolar backbone and the polar ionic groups. In addition to current applications ranging from thermoplastic elastomers to selective ion-transport membranes, ionomers have potential to enable the next generation of polymeric electrolytes for fuel cell and battery applications. To date, studies of the structure and properties of ionomers have focused on materials with poorly defined macromolecular architectures because of synthetic limitations as well as a focus on commercially relevant highly branched, random ionomers. Random ionomers typically have ionic aggregates dispersed with liquidlike order in an amorphous or semicrystalline matrix; however, the wide distribution in aggregate separation leads to broad scattering features which complicate efforts to draw quantitative conclusions about aggregate composition. A recent review of the hierarchical morphology of ionomers identified the effect of precise functional group spacing on ionomer morphology and properties as an open question.[1] In this paper, we demonstrate that precise ionomers yield more uniform aggregate distributions with better defined scattering features, and in one case, the precision leads to the self-assembly of ionic aggregates onto a lattice, as routinely observed in block copolymers.

Ionomer systems with varying degrees of control over functional group spacing have been investigated. Halato-telechelic polymers are linear or star polymers with low polydispersity that have ionic groups only at the chain ends; thus, they have a much more precise structure than typical ionomers but the acid group spacing is still not perfectly monodisperse. Additionally, restricting the acid groups to chain ends limits their acid content and complicates their use a model systems for the behavior of typical ionomers.[2] Polyurethane-based ionomers yield some control over functional group spacing because ionic groups are only attached at the polyurethane linkages. The length of the polyols separating the linkages can be controlled and can have modest polydispersities (<1.5).[3,4] However, the functional group spacing is not monodisperse, and the backbone can be thought of as a segmented copolymer which may influence the morphology. Ionenes or polymers, where the ionic groups are incorporated into the chain backbone rather than being pendant moieties, have been produced with monodisperse ammonium spacing along the backbone.[5] However, incorporation of charged groups into the backbone rather than as pendant moieties results in chains that are segmented

[†] Department of Materials Science and Engineering, University of Pennsylvania.
[‡] Department of Chemical and Biomolecular Engineering, University of Pennsylvania.
[§] Current address: DuPont Experimental Station, Wilmington, DE.
[⊥] Department of Chemistry, University of Florida.
[¶] Current address: DSM, Geleen, the Netherlands.

(1) Grady, B. P. *Polym. Eng. Sci.* **2008**, *48*, 1029.
(2) Vanhoorne, P.; Jerome, R. In *Ionomers: Characterization, Theory, and Applications*; Schlick, S., Ed.; CRC: Boca Raton, FL, 1995, p 187.
(3) Visser, S. A.; Cooper, S. L. *Macromolecules* **1991**, *24*, 2584.
(4) Visser, S. A.; Cooper, S. L. *Polymer* **1992**, *33*, 920.
(5) Williams, S. R.; Borgerding, E. M.; Layman, J. M.; Wang, W.; Winey, K. I.; Long, T. E. *Macromolecules* **2008**, *41*, 5216.

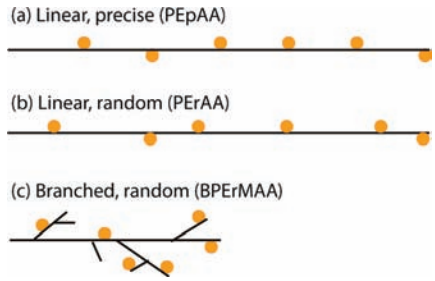

Figure 1. Schematic of copolymers used in this study where circles indicate acid groups. Linear poly(ethylene-*co*-acrylic acid) copolymers with (a) acid groups separated by a precisely controlled number of carbon atoms synthesized via ADMET and (b) acid groups with pseudorandom spacings synthesized via ROMP. (c) Branched poly(ethylene-*ran*-methacrylic acid) copolymers with randomly spaced acid groups commercially produced using high-pressure polymerization. Note that all materials are atactic and are drawn with the same acid content.

copolymers. This drives microphase separation and makes ionenes a distinctly different class of material from ionomers.[6]

Recently advances in acyclic diene methathesis (ADMET) chemistry and ring-opening metathesis polymerization (ROMP) has enabled production of linear polyethylenes with, respectively, either precisely controlled or pseudorandom placement of functional groups such as halogens,[7−9] alkyl chains,[10] and acid groups.[11,12] Neutralizing poly(ethylene-*co*-acrylic acid) copolymers with precise acid group spacing synthesized via ADMET with a metallic salt produces ionomers with unparalleled control of acid position along the chain without the complications of segmented backbones. Neutralization also ensures that there is sufficiently high electron density contrast for X-ray scattering and scanning transmission electron microscopy (STEM) to yield quantitative morphological information.

The present study investigates the effect of chain architecture (linear vs branched), acid placement (precise vs random), acid content, neutralization extent, and crystallinity on the morphology of poly(ethylene-*co*-acrylic acid)−Zn and poly(ethylene-*ran*-methacrylic acid)−Zn ionomers. The materials investigated are summarized in Figure 1 and Table 1. High angle annular dark field scanning transmission electron microscopy (HAADF-STEM) was used to directly image the ionic aggregates and verify the validity of the model used to extract quantitative morphological information from the X-ray scattering data. Differential scanning calorimetry (DSC) was used to determine which materials are semicrystalline. X-ray scattering from drawn samples and samples at elevated temperature allows the scattering contributions from acid layers associated with crystallites and ionic aggregates dispersed in the amorphous phase to be separated for semicrystalline precise ionomers. Comparison of precise and random linear ionomers with identical acid content and neutralization level demonstrates that precisely controlled acid spacing leads to much more intense and well-defined scattering peaks indicating a greatly reduced polydispersity in correlation lengths between ionic aggregates. In consequence, morphological parameters can be extracted from scattering models with more confidence. Moreover, the ionic aggregates of a precise amorphous ionomers with 22 mol % acid self-assemble with cubic ordering. By comparing precise ionomers in the fully amorphous state, we will be able to draw conclusions about how acid content, neutralization level, and acid placement affect the size and distribution of ionic aggregates. We conclude with a discussion of how this new family of precise ionomers yields more insight into the composition of the ionic aggregates.

Background. A broad scattering peak is generally observed at scattering vector (q) $\approx 1-5$ nm^{-1} in ionomers and is referred to as the "ionomer peak."[13−15] This feature has been attributed to interaggregate scattering, and the Yarusso−Cooper[15] (YC) and Kinning−Thomas[16] (KT) models are widely used to fit the ionomer peak and gain insight into the composition of the aggregates.[3,14,15,17] These models treat the ionic aggregates as monodisperse hard spheres distributed with liquidlike order in a uniform matrix. The model parameters include the radius of the aggregate (R_1), the radius of closest approach (R_{CA}) that limits the spatial correlation between aggregates, the number density of aggregates (N_p) (note that $N_p = 1/V_p$ where V_p is the average sample volume per aggregate), and the peak amplitude. The models differ in their correlation functions; the YC model uses the Fournet three-body correlation function,[18] whereas the KT model uses the Percus−Yevick correlation function[19] that accounts for interference from all of the particles in the system. Therefore, the KT is more accurate for systems with a high density of particles. Details of[15,16] and comparison between[20] these models can be found in the literature. Adhesive interactions between the hard spheres have also been included in order to capture the low q upturn often observed for ionomers; however, this model is less successful in capturing the ionomer peak.[3] It should be noted that because this scattering feature is relatively broad and weak, scattering models based on intraparticle interference[21−23] have also been proposed to account for the ionomer peak; however, there is general consensus in the community that interaggregate scattering is more likely responsible.[3,24]

The assumptions of the YC and KT models have been shown to be consistent with STEM direct imaging of ionic aggregates for some ionomer systems. However, ionic aggregates can have a variety of shapes and distributions,[25] and thus these models are not appropriate for all ionomers. It is imperative to use a direct imaging method to confirm that aggregate morphology

(6) Hashimoto, T.; Sakurai, S.; Morimoto, M.; Nomura, S.; Kohjiya, S.; Kodaira, T. *Polymer* **1994**, *35*, 2672.
(7) Alamo, R. G.; Jeon, K.; Smith, R. L.; Boz, E.; Wagener, K. B.; Bockstaller, M. R. *Macromolecules* **2008**, *41*, 7141.
(8) Boz, E.; Nemeth, A. J.; Ghiviriga, I.; Jeon, K.; Alamo, R. G.; Wagener, K. B. *Macromolecules* **2007**, *40*, 6545.
(9) Boz, E.; Wagener, K. B.; Ghosal, A.; Fu, R. Q.; Alamo, R. G. *Macromolecules* **2006**, *39*, 4437.
(10) Sworen, J. C.; Wagener, K. B. *Macromolecules* **2007**, *40*, 4414.
(11) Baughman, T. W.; Chan, C. D.; Winey, K. I.; Wagener, K. B. *Macromolecules* **2007**, *40*, 6564.
(12) Valenti, D. J.; Wagener, K. B. *Macromolecules* **1998**, *31*, 2764.
(13) Benetatos, N. M.; Winey, K. I. *J. Polym. Sci., Part B: Polym. Phys.* **2005**, *43*, 3549.
(14) Kutsumizu, S.; Tagawa, H.; Muroga, Y.; Yano, S. *Macromolecules* **2000**, *33*, 3818.
(15) Yarusso, D.; Cooper, S. L. *Polymer* **1985**, *26*, 371.
(16) Kinning, D. J.; Thomas, E. L. *Macromolecules* **1984**, *17*, 1712.
(17) Tsujita, Y.; Yasuda, M.; Takei, M.; Kinoshita, T.; Takizawa, A.; Yoshimizu, H. *Macromolecules* **2001**, *34*, 2220.
(18) Fournet, G. *Acta Crystallogr.* **1951**, *4*, 293.
(19) Percus, J. K.; Yevick, G. J. *Phys. Rev.* **1958**, *110*, 1.
(20) Zhou, N. C.; Chan, C. D.; Winey, K. I. *Macromolecules* **2008**, *41*, 6134.
(21) Roche, E. J.; Stein, R. S.; Russell, T. P.; Macknight, W. J. *J. Polym. Sci.: Polym. Phys. Ed.* **1980**, *18*, 1497.
(22) Fujimura, M.; Hashimoto, T.; Kawai, H. *Macromolecules* **1981**, *14*, 1309.
(23) MacKnight, W. J. T., W. P.; Stein, R. S. *J. Polym. Sci. Symp.* **1974**, *45*, 113.
(24) Eisenberg, A.; Kim, J.-S. *Introduction to Ionomers*, 1st ed.; Wiley: New York, 1998.
(25) Batra, A.; Cohen, C.; Kim, H.; Winey, K. I. *Macromolecules* **2006**, *39*, 1630.

Table 1. Summary of Ionomers Studied

name	polymerization technique	acid placement	backbone architecture	mol % acid	extent of Zn neutralization, %
$PEpAA_{9.5}$	ADMET	precise	linear	9.5	0, 56, 86, 116
$PEpAA_{13}$	ADMET	precise	linear	13.3	0, 82
$PEpAA_{22}$	ADMET	precise	linear	22.2	0, 66
$PErAA_{13}$	ROMP	pseudorandom	linear	13.3	0, 18, 81
$BPErMAA_4$	high-pressure polymerization	random	branched	~4	0, 29, 55, 78

and distribution is consistent with model assumptions. While STEM can be used to determine aggregate size, shape, and global uniformity, the number density of aggregates cannot be determined without performing three-dimensional (3D) modeling to correct for extensive feature overlap in the STEM projections.[26] Quantitative agreement between STEM and X-ray scattering has been demonstrated for poly(styrene-*ran*-7.2%-methacrylic acid) neutralized by Cu[26,27] and poly(styrene-*ran*-1.9%-sulfonated styrene) neutralized by Zn, Ba, Cs, and Cu.[20]

In the mid-1960s, ionomers based on branched, random poly(ethylene-*ran*-methacrylic acid) copolymers (BPErMAA) with structure similar to that of low-density PE[1] were developed and became commercially important due to their excellent mechanical and chemical stability. While BPErMAA materials have been neutralized with a variety of mono- and divalent cations, the following discussion focuses on zinc-neutralized materials. Their morphology has been investigated via X-ray scattering[13−15,17,28] and atomic force microscopy,[29] while the local structure of the ionic aggregates has been studied using Fourier transform infrared spectroscopy (FTIR)[30,31] as well as X-ray absorption spectroscopy.[1] Direct imaging with HAADF-STEM shows a liquidlike distribution of roughly circular ion-rich features (see Figure 2d) with diameters ~2 nm.[32,33] The image interpretation of these materials is complicated by their hierarchical morphology which includes PE crystallites as well as amorphous regions in which ionic aggregates are dispersed. Similarly, their X-ray scattering patterns show features at a variety of length scales. At wide angle (high q), there is an amorphous halo at $q \approx 12-16$ nm^{-1} related to the average backbone−backbone spacing as well as reflections from the PE crystallites. At intermediate angles, there is a broad peak centered around $q \approx 3$ nm^{-1} which is absent in the acid form.[13−15] For zinc-neutralized materials, the ionomer peak is relatively weak and broad compared to that from other ionomer systems, making it difficult to quantitatively fit. At small angles ($q \approx 0.4$ nm^{-1}), a peak associated with the average lamellae−lamellae spacing is observed. There is also a low q upturn seen in neutralized materials that is generally attributed to large-scale inhomogeneities in the distribution of aggregates.[34,35]

Recently, synthetic advances have allowed for the production of high-molecular-weight linear poly(ethylene-*co*-acrylic acid) (PEpAA) with precisely sequenced acid groups or a pseudo-random distribution of acid groups (PErAA) (see Figure 1).[11] PErAA materials behave similarly to commercial BPErMAA materials in that the overall crystallinity increases with decreasing acid content and the scattering features are those associated with semicrystalline PE.[11] In contrast, PEpAA materials have additional features at intermediate angles. Materials with an acid group on every 21st carbon, $PEpAA_{9.5}$, are semicrystalline and exhibit a series of sharp peaks at $q = 2.48$, 4.81, and 7.55 nm^{-1} (see reference 11 and Figure 3a). These features are consistent with a layered structure with repeat distances of 2.53 nm. Aligning samples via stretching reveals that the planes containing the acid groups orient perpendicular to the draw direction. Thus, these semicrystalline precise materials have layers of dimerized acids associated with the crystallites that orient perpendicular to the chain backbones. As the acid content is increased, PEpAA materials become amorphous. For $PEpAA_{13}$ and $PEpAA_{22}$ materials with acid groups on every 15th or ninth carbon, a weak, broad peak is observed at $q = 4.4$ and 6.4 nm^{-1}, respectively (see reference 11 and Figure 3a). These broad features arise from correlations between the acid dimers distributed in the amorphous matrix. This feature is absent in materials with random acid spacing because the positions of the acid dimers are uncorrelated.

Results and Discussion

Direct Imaging of Ionic Aggregates. HAADF-STEM was used to verify the shape and spatial distribution of the ionic aggregates

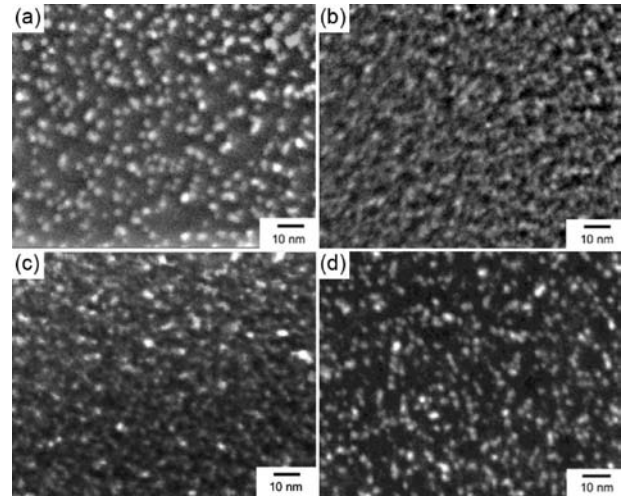

Figure 2. HAADF-STEM micrographs from (a) $PEpAA_{9.5}$−Zn56, (b) $PEpAA_{13}$−Zn82, (c) $PEpAA_{9.5}$−Zn86, and (d) $BPErMAA_4$−Zn55 (adapted from Laurer and Winey[32]). Scale bars are 10 nm. Ionic aggregates, that appear light, are roughly circular and distributed in a liquidlike fashion throughout the sample.

(26) Benetatos, N. M.; Chan, C. D.; Winey, K. I. *Macromolecules* **2007**, *40*, 1081.
(27) Benetatos, N. M.; Heiney, P. A.; Winey, K. I. *Macromolecules* **2006**, *39*, 5174.
(28) Loo, Y.-L.; Wakabayashi, K.; Huang, Y. E.; Register, R. A.; Hsiao, B. S. *Polymer* **2005**, *46*, 5118.
(29) Sauer, B. B.; McLean, R. S. *Macromolecules* **2000**, *33*, 7939.
(30) Coleman, M. M.; Lee, J. Y.; Painter, P. C. *Macromolecules* **1990**, *23*, 2339.
(31) Walters, R. M.; Sohn, K. E.; Winey, K. I.; Composto, R. J. *J. Polym. Sci., Part B: Polym. Phys.* **2002**, *41*, 2833.
(32) Laurer, J. H.; Winey, K. I. *Macromolecules* **1998**, *31*, 9106.
(33) Winey, K. I.; Laurer, J. H.; Kirkmeyer, B. P. *Macromolecules* **2000**, *33*, 507.
(34) Ding, Y. S.; Hubbard, S. R.; Hodgson, K. O.; Register, R. A.; Cooper, S. L. *Macromolecules* **1988**, *21*, 1698.

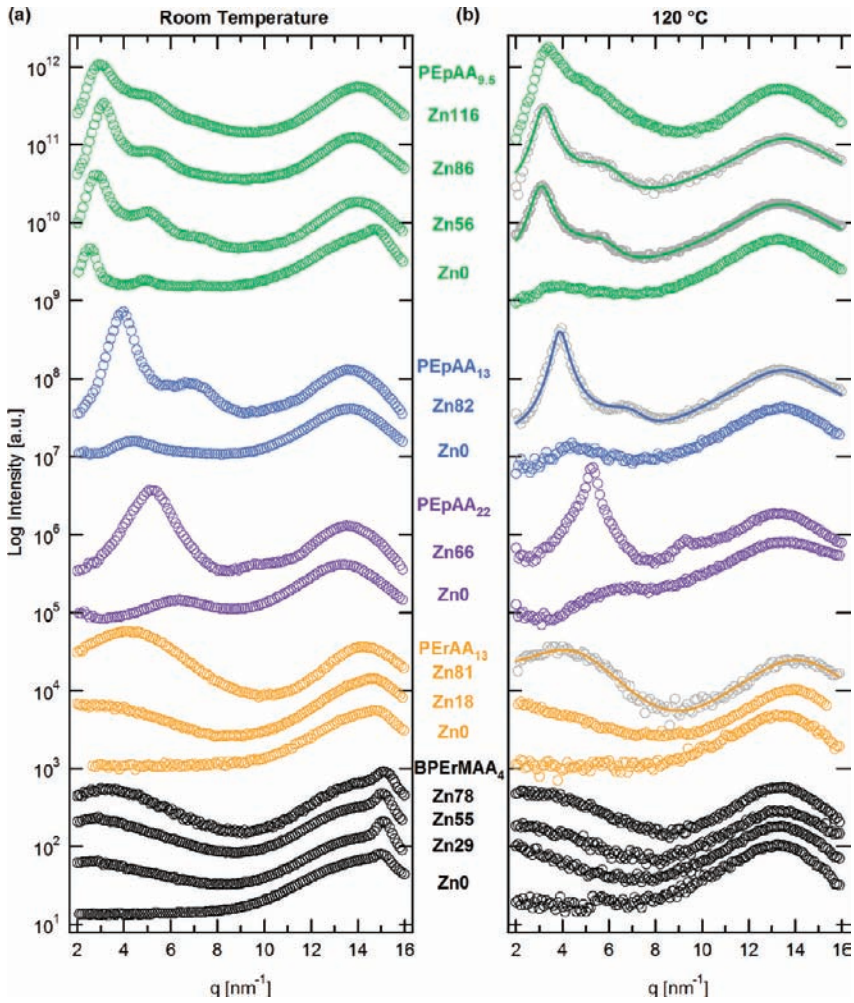

Figure 3. Isotropic X-ray scattering data at (a) room temperature and (b) 120 °C. The intensities are normalized to the amorphous peak at 13.6 nm^{-1} before being vertically shifted for clarity. Experimental data are shown as open circles, while fits to selected scattering data using the KT model for the ionomer peak and a Lorenzian function for the amorphous PE halo are shown as solid lines.

as some ionomers can have highly nonuniform ionic aggregate distributions[36] or can exhibit multiple aggregate shapes.[25,37] In HAADF-STEM, ionic aggregates with higher average atomic number appear light while the polymer matrix appears dark. Depending on the concentration of ionic aggregates and the sample thickness, the bright features can either correspond to individual ionic aggregates in relatively dilute systems or to areas in which multiple ionic aggregates overlap due to projection through the sample. Previous image simulations of ionomers have demonstrated that the extent of overlap is significant due to the small ionic aggregate size, high concentration of aggregates and the specimen thickness.[26] Interestingly, the overlaps does not substantially distort the average feature size or shape. Figure 2 shows representative HAADF-STEM images. All materials imaged resulted in similar micrographs and images collected at different areas of the samples indicate a globally uniform microstructure (e.g., there are no regions devoid of aggregates). Moreover, all samples show a morphology consistent with the assumptions of the KT model of liquid packing of monodisperse spherical aggregates. There is no significant difference in aggregate size or shape as a function of acid distribution, backbone linearity, or neutralization extent, which is consistent with the work of Laurer and Winey[32,33] on branched poly(ethylene-*ran*-methacrylic acid)−Zn ionomers. The spatial distribution of ionic aggregates is consistent with image simulations of spherical objects with liquidlike order.[26] Thus, while the STEM images suggest the KT model would be appropriate for modeling the scattering from the ionic aggregates in these systems, they do not provide all of the relevant model parameters. Additionally, these STEM images do not differentiate between amorphous and crystalline regions in the materials.

Differential Scanning Calorimetry. To determine whether samples are semicrystalline or amorphous at room temperature, DSC experiments were performed. For PEpAA$_{9.5}$ materials with acid groups on every 21st carbon, crystallinity decreases with increasing neutralization level until reaching full neutralization where no crystallinity is detected via DSC (see Table 2). This is similar to that of branched semicrystalline ionomers where increased neutralization decreases crystallinity at short aging times.[38] Precise, linear materials with acid spacing less than 20 carbons, that is PEpAA$_{13}$ and PEpAA$_{22}$ with higher acid contents, show no melting endotherm.[11] This suggests that PE sequences must be longer than 14 carbons to crystallize.

(35) Williams, C. E.; Russell, T. P.; Jerome, R.; Horrion, J. *Macromolecules* **1986**, *19*, 2877.
(36) Taubert, A.; Winey, K. I. *Macromolecules* **2002**, *35*, 7419.
(37) Kirkmeyer, B. P.; Weiss, R. A.; Winey, K. I. *J. Polym. Sci., Part B: Polym. Phys.* **2001**, *39*, 477.
(38) Wakabayashi, K.; Register, R. A. *Macromolecules* **2006**, *39*, 1079.

Table 2. DSC Results

material	% Zn	T_m (°C)	ΔH_m (J/g)
$PEpAA_{9.5}$	0	45.6	52.8
	56	52.8	16.2
	82	59.5	4.9
	116	N/A	N/A
$PEpAA_{13}$	0	N/A[a]	N/A[a]
	82	N/A	N/A
$PEpAA_{22}$	0	N/A[a]	N/A[a]
	66	N/A	N/A
$PErAA_{13}$	0	74[a]	51[a]

[a] Data from Baughman et al.[11]

Similarly, pseudorandom linear materials with 22 mol % acid are amorphous, but lower acid content materials become increasingly crystalline as the acid content decreases.[11] While $PEpAA_{13}$ and $PErAA_{13}$ have the same concentration of acid groups, the former is amorphous, and the latter is semicrystalline. Due to its precise nature, $PEpAA_{13}$ contains no PE sequences longer than 14 carbons, while the random acid placement in $PErAA_{13}$ results in some longer PE sequences that are able to crystallize. It should be noted that branched BPErMAA copolymers with 13 mol % acid are amorphous;[14] thus, linear copolymers are able to retain crystallinity at higher acid content as they lack branch points. Consistent with previous literature,[39] the $BPErMAA_4$−Zn ionomers used in this study are all expected to be semicrystalline at room temperature.

X-ray Scattering

Room Temperature X-ray Scattering from Isotropic Samples. The X-ray scattering patterns collected at room temperature from hot pressed and rapidly cooled samples are shown in Figure 3a. All patterns are isotropic and were azimuthally integrated to generate intensity versus q plots. The amorphous PE halo at $q \approx 13.6$ nm^{-1} was used to normalize the relative intensities.

It is immediately clear from Figure 3a that ionomers with the same acid content but different acid spacing ($PErAA_{13}$−Zn and $PEpAA_{13}$−Zn82) give rise to dramatically different scattering curves (see Supporting Information, Figure S1 for a detailed comparison). By precisely controlling the acid group separation, the ionomer peak is much more intense and well-defined. However, it should be noted that at room temperature $PErAA_{13}$−Zn18 is semicrystalline, while $PEpAA_{13}$−Zn82 is amorphous, complicating the direct comparison of the effect of acid placement.

Let us focus on the crystalline reflection at $q \approx 15$ nm^{-1} associated with PE crystallites. Crystallinity is easily discerned in $BPErMAA_4$ materials both in the acid and neutralized forms as expected for these materials. Consistent with the DSC results, this reflection is observed for $PErAA_{13}$−Zn0 and persists after neutralization with 18% Zn. For linear, precise materials with high acid content ($PEpAA_{13}$ and $PEpAA_{22}$), which DSC results suggest are amorphous, no high angle reflection is observed in either the acid or neutralized form. In the lowest acid content precise material, $PEpAA_{9.5}$, this reflection is observed in the acid form but is either absent or difficult to discern in $PEpAA_{9.5}$−Zn ionomers. This is consistent with the decrease in melting enthalpy with increasing neutralization detected via DSC (Table 2).

Scattering features at $q \approx 2-10$ nm^{-1} in ionomers have traditionally been associated with interaggregate scattering from the ionic aggregates dispersed in the amorphous regions. It is clear that, for all systems, features at $q \approx 2-10$ nm^{-1} either appear or are strengthened as the acid forms are neutralized with zinc, Figure 3. For both linear and branched materials with random acid spacing, this region is featureless in the acid form due to uncorrelated positions of the acid dimers along the polymer backbone. However, with neutralization a single broad scattering feature center at $q \approx 3-4$ nm^{-1} is observed for $PErAA_{13}$−Zn and $BPErMAA_4$−Zn ionomers. As the extent of neutralizing increases for $BPErMAA_4$−Zn and $PErAA_{13}$−Zn ionomers, the peak becomes somewhat more intense and shifts toward slightly higher q. For linear precise $PEpAA_{13}$−Zn82 and $PEpAA_{22}$−Zn66, which are amorphous, neutralization with ∼75% zinc greatly increases the intensity of the peak in this range and shifts its position to *lower* q relative to the peak observed in the acid form (from $q = 4.4$ to 4.0 nm^{-1} and $q = 6.4$ to 5.3 nm^{-1}, respectively). For $PEpAA_{13}$−Zn82 a second peak at $q = 7.0$ nm^{-1} is also observed.

Scattering from $PEpAA_{9.5}$−Zn ionomers differs significantly from the other systems. The strongest peak at $q^* \approx 2.5$ nm^{-1} shifts to slightly *higher* q with increasing neutralization and the well-defined second peak located at $2q^*$ in the acid form shifts to lower q than $2q^*$. As discussed above, in $PEpAA_{9.5}$−Zn0 the peaks between $q \approx 2.5-10$ nm^{-1} are attributed to layers of dimerized acids arranged perpendicular to the chain backbones. As this material is neutralized with zinc, spherical ionic aggregates are formed as confirmed via STEM, and crystallinity is greatly reduced. If the scattering from this region is dominated by crystallinity effects in $PEpAA_{9.5}$−Zn0, it is not expected that the peaks observed for the amorphous $PEpAA_{9.5}$−Zn116 would have the same origin. Scattering from semicrystalline $PEpAA_{9.5}$−Zn materials most likely contains contributions from both the layered acid structure associated with crystallites and from interaggregate scattering from ionic aggregates dispersed in the amorphous regions. However, as these contributions overlap in the scattering vector and the extent of crystallinity changes upon neutralization, it is not possible to deconvolute their relative contributions to the scattering simply via a peak subtraction method.

X-ray Scattering from Drawn Samples. Alignment of crystallites via drawing is a useful method of determining what features are associated with crystalline or amorphous regions of a sample. To that end, samples were heated until soft and stretched to induce alignment. Figure 4 shows 2D scattering patterns, corresponding to a q range of ∼2−20 nm^{-1}, collected from aligned samples at room temperature. The stretching direction is indicated by the arrows. It should be noted that no induced anisotropy is expected for amorphous materials at these relatively low strain rates, and $PEpAA_{13}$−Zn0 and $PEpAA_{13}$−Zn82 remain isotropic as expected (**4a** and **4b**). For semicrystalline $PErAA_{13}$−Zn0 (**4c**) and $BPErMAA_4$−Zn0 (**4e**) that have random acid placement, the crystalline reflection (near the edge of the detector) becomes anisotropic and orients perpendicular to the drawing direction, indicating chain backbones are aligned along the draw direction. When these materials are neutralized and stretched (**4d** and **4f**) the crystalline reflection is anisotropic; however, the ionomer peak (near the beam stop) is isotropic indicating no alignment of the ionic aggregates in the amorphous regions. This is consistent with previous observations in blown films of $BPErMAA_4$−Zn ionomers where both STEM and X-ray scattering indicated no change in aggregate size, shape, or distribution with increasing blow ratio, although the PE crystals were anisotropic.[13]

(39) Eisaku, H.; Yoshimasa, Y.; Kenji, T.; Shinichi, Y. *J. Appl. Polym. Sci.* **1991**, *42*, 351.

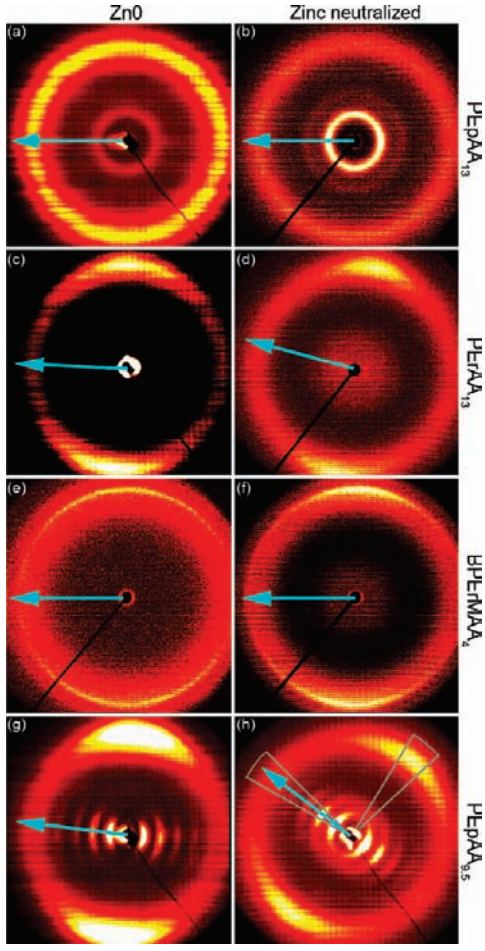

Figure 4. Two-dimensional (2D) X-ray scattering patterns for oriented (a) $PEpAA_{13}$−Zn0, (b) $PEpAA_{13}$−Zn82, (c) $PErAA_{13}$−Zn0, (d) $PErAA_{13}$−Zn18, (e) $BPErMAA_4$−Zn0, (f) $BPErMAA_4$−Zn29, (g) $PEpAA_{9.5}$−Zn0, and (h) $PEpAA_{9.5}$−Zn56. Patterns correspond to a q range of ∼2−20 nm^{-1}, and arrows indicate the draw direction. The angular range azimuthally integrated to generate the 1D intensity vs q plots in Figure 5 are shown in image h.

The semicrystalline $PEpAA_{9.5}$ materials (**4g** and **4h**) show a strikingly different behavior when stretched. In these materials, both the crystalline PE reflection and the low q features become anisotropic. To more clearly investigate this behavior, images a and b of Figures 5 plot, respectively, the intensity versus q perpendicular and parallel to the drawing direction as a function of neutralization level. Parallel to the draw direction (**5b**), all samples except the fully neutralized material show at least four peaks at positions consistent with integer multiples of the first peak position, indicating a highly regular layered structure perpendicular to the polymer chain. We attribute these scattering features to acid dimers decorating the crystalline lamellae wherein the acid−acid separation is well-defined due to the precise acid placement. The peak positions are in agreement with an all-*trans* PE conformation of 20 carbons, and the peak intensity decreases as the percent crystallinity decreases with increasing levels of neutralization. In fact, for the fully neutralized $PEpAA_{9.5}$−Zn116, the first peak is shifted to higher q relative to those of the other samples, and the peak positions are less consistent with a layered structure, suggesting much less ordering in this material which DSC indicates is amorphous. If $PEpAA_{9.5}$−Zn116 is amorphous, it should be unaffected by drawing; however, the weak anisotropy observed in this sample may be due to strain-induced crystallization. Perpendicular to

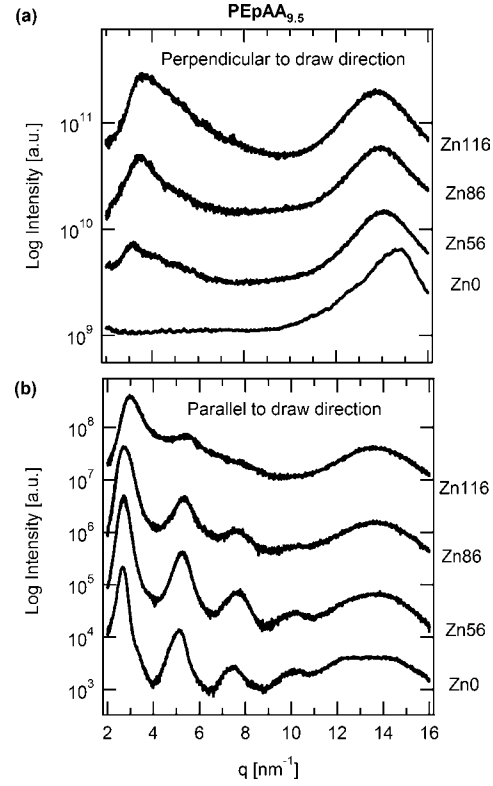

Figure 5. Intensity versus q (a) perpendicular and (b) parallel to the draw direction for stretched $PEpAA_{9.5}$−Zn ionomers. Patterns were azimuthally integrated over the angular regions indicated in Figure 4h. The intensities are normalized to the amorphous peak at 13.6 nm^{-1} before being vertically shifted for clarity.

the draw direction (**5a**), $PEpAA_{9.5}$−Zn0 is featureless at low q. In contrast, all the neutralized materials show a peak at $q \approx 3-4$ nm^{-1} that shifts toward higher q and increases in intensity with increasing neutralization level. Thus, scattering in this region perpendicular to the drawing direction is apparently dominated by ionic aggregates dispersed in the amorphous phase. Therefore, scattering features in the angular region $q \approx 2-10$ nm^{-1} (the green curves in Figure 3a) for pressed $PEpAA_{9.5}$−Zn ionomers are due to a superposition of contributions from the acid layers and from the ionic aggregates. The results from drawn samples suggest that orienting samples via drawing leads to some deconvolution of contributions from crystallites and from ionic aggregates; however, this can only be definitively determined if one of the contributions can be entirely removed. To this end, scattering patterns were collected at 120 °C which is well above the melting points of the crystallites; these results are discussed below.

X-ray Scattering at High Temperature from Amorphous Samples. Scattering patterns collected at 120 °C, where all samples are fully amorphous, are shown in Figure 3b. Upon heating, the crystalline reflections at $q \approx 15$ nm^{-1} are no longer observed for any materials, and the amorphous halo shifts very slightly toward lower q due to thermal expansion.

By rendering all samples amorphous via heating, we remove any possible effects due to differing crystallinity and are now in a position to isolate the effect of the distribution of acid groups along linear PE molecules. Figure 6 plots scattering intensity versus q for $PEpAA_{13}$ and $PErAA_{13}$ in the unneutralized and neutralized states at 120 °C. *The linear intensity scale makes clear the dramatically sharper and more intense features for neutralized ionomers with precise rather than random acid*

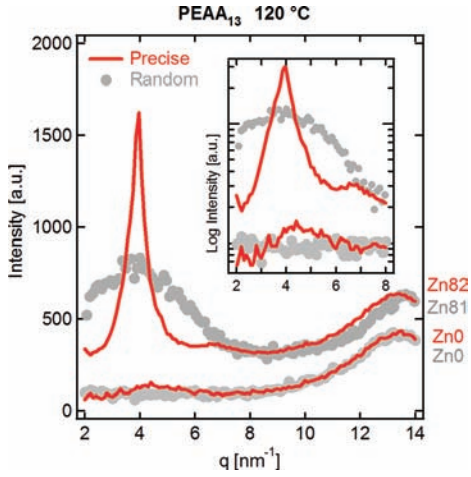

Figure 6. Scattering intensity versus q for $PEpAA_{13}$−Zn0, $PEpAA_{13}$−Zn82, $PErAA_{13}$−Zn0, and $PErAA_{13}$−Zn81 at 120 °C plotted on a linear scale. The inset shows the low q features on a log scale. Moving from an ionomer with a pseudorandom acid distribution to a precise distribution dramatically increases the intensity of the ionomer peak. The more intense and well-defined peak indicates that the spatial distribution of the ionic aggregates is vastly more uniform in precise ionomers.

spacing. The low-angle ionomer peaks for $PEpAA_{13}$−Zn82 and $PErAA_{13}$−Zn81 are, respectively, ∼3.4 and 1.3 times as intense as the amorphous halo. The more intense and well-defined peak indicates that the spatial distribution of the ionic aggregates is more uniform in precise materials. Implications of the reduced morphological variability for extracting quantitative information about aggregate size and distribution will be discussed in the next section.

To understand the effect of temperature on materials with precisely spaced acids, let us begin by considering their behavior in the unneutralized state. For $PEpAA_{13}$−Zn0 and $PEpAA_{22}$−Zn0, which are amorphous at room temperature, no significant changes upon heating are observed (Figure 3). In contrast, $PEpAA_{9.5}$−Zn0 shows significant structural evolution on heating with the sharp peaks associated with the layered acid structure merging into a weak, broad peak centered at $q \approx 4$ nm^{-1}. This structural transition is complete by ∼58 °C (see Supporting Information, Figure S2) which correlates with the endotherm observed via DSC.[11] This is consistent with a loss of the layered ordering of the acid groups due to melting of the crystallites. In the amorphous state, precise materials with acid groups on every 9th, 15th, or 21st carbon have peaks respectively at $q = 6.4$, 4.4, and 4 nm^{-1}, corresponding to Bragg spacings of 1.0, 1.4, and 1.6 nm. The increase in spacing with increasing acid separation suggests that these features are related to the average acid dimer separation in an amorphous PE matrix. By precisely controlling the acid spacing along the polymer backbone, the interacid dimer correlations, which are absent in materials with randomly distributed acid groups, are observed both in the semicrystalline and amorphous states for unneutralized materials.

By comparing the three precise ionomers in the fully amorphous state (120 °C), Figure 3b, it is clear that neutralization affects the low-angle scattering features similarly: peak intensity increases, a secondary peak appears, and the strongest peak shifts to lower q relative to the peak observed in the unneutralized material. The shift to lower q suggests that the scattering centers are further apart in the neutralized material as compared to those of the acid form. This is consistent with partial neutralization. As neutralization drives the formation of ionic aggregates, the average distance between scattering centers increases relative to the acid dimers.

Heating does not affect the position of the low-angle features for either $PEpAA_{13}$−Zn82 or $PEpAA_{22}$−Zn66 as expected for amorphous materials that undergo no structural transformation on heating (the ionic aggregates persist to temperatures well above 120 °C for these types of ionomers).[15,40] In contrast, heating affects the scattering observed for all the neutralized $PEpAA_{9.5}$ materials because these ionomers are semicrystalline at room temperature and amorphous at 120 °C. Figure 7 directly compares the scattering from $PEpAA_{9.5}$−Zn0 and $PEpAA_{9.5}$−Zn56 at room temperature and 120 °C. After heating, the high q reflection due to the PE crystallites is absent, the amorphous halo shifts toward lower q due to thermal expansion, and the location of the strongest peaks for $PEpAA_{9.5}$−Zn shifts from $q \approx 2.5-3$ nm^{-1} to $\sim 3-3.5$ nm^{-1}. At low temperature, features observed at $q \approx 2-10$ nm^{-1} have contributions from both interaggregate scattering and from the ordered acid structure associated with the crystalline regions. In contrast, at high temperature, features in this region arise solely from interaggregate scattering. The scattering patterns collected at high temperature are very similar to what is observed perpendicular to the drawing direction in oriented samples both in terms of peak location and overall pattern shape (see Figure 5b and Supporting Information, Figure S3). Thus, the assumption that scattering perpendicular to the drawing direction results primarily from ionic aggregates dispersed in the amorphous phase is further substantiated. These results suggest that additional care is necessary when analyzing the scattering from semicrystalline ionomers with precisely spaced functional groups in order to differentiate between interaggregate scattering and scattering from functional groups associated with crystalline regions.

Scattering patterns evolve with temperature for $BPErMAA_4$−Zn and $PErAA_{13}$−Zn18 materials that have randomly distributed acid groups and are semicrystalline at room temperature (Figure 3b). At 120 °C the broad ionomer peak shifts toward lower q compared to the situation at room temperature. Moreover, as this scattering feature shifts, it begins to overlap with the low-q upturn, making the peak maximum difficult to identify with confidence (see Supporting Information Figures S6 and S4). This shift could be related to the release of PE segments from crystallites into the amorphous matrix which effectively dilutes the number density ionic aggregates.[15]

Modeling X-ray Patterns and Precise Ionomer Morphology. By investigating the materials in the fully amorphous state, we are now in a position to obtain quantitative information about the size and separation of the ionic aggregates in these precise ionomers by using the KT model. The scattering intensity patterns collected at 120 °C were fit using a multifunction model

$$I(q) = I_{KT}(q) + I_L(q) + C \qquad (1)$$

where $I_{KT}(q)$ is the contribution from the KT model to describe the intermediate angle scattering, $I_L(q)$ is a Lorenzian function to model the amorphous halo at wide angle, and C is a constant to account for the background.[20,26] Resulting fits for four ionomers are shown as solid lines in Figure 3b. It is clear that the KT model fits $PEpAA_{13}$−Zn82, $PEpAA_{9.5}$−Zn56, $PEpAA_{9.5}$−Zn86, and $PErAA_{13}$−Zn81 ionomers in the amorphous state, lending further evidence that the ionomer peak arises from interparticle interference. We do not include a fit to

(40) Vanhoorne, P.; Register, R. A. *Macromolecules* **1996**, *29*, 598.

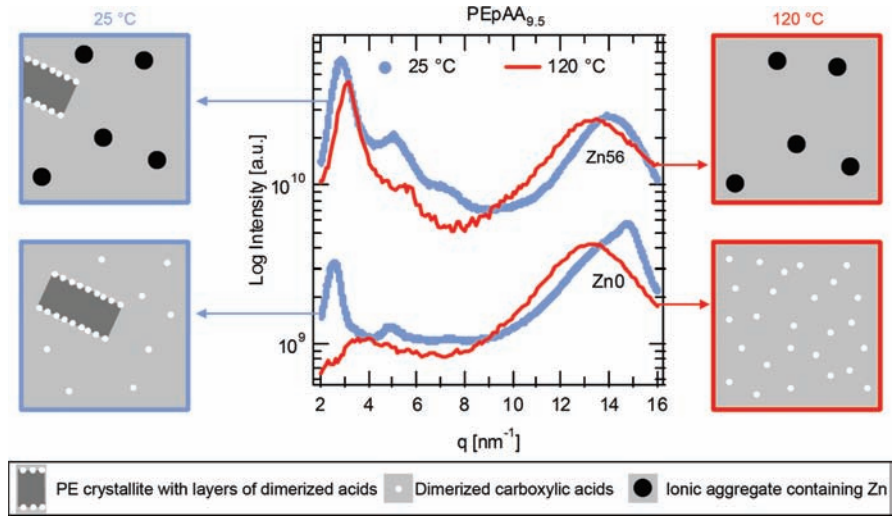

Figure 7. Comparison of scattering curves at room temperature and 120 °C for $PEpAA_{9.5}$−Zn0 and $PEpAA_{9.5}$−Zn56. Also included are schematics illustrating the morphological features giving rise to the scattering peaks. The high q peak shifts toward lower q as the crystallites melt and the material thermally expands. Heating $PEpAA_{9.5}$−Zn0 causes the sharp, low-q peaks arising from the layered acid structure associated with the crystallites to merge into a broad peak arising from the correlated dimer positions in the amorphous phase. The low-q features for $PEpAA_{9.5}$−Zn56 shift on heating as contributions from the layered acid structure are lost and interaggregate scattering from ionic aggregates dispersed in the amorphous phase dominates at high temperature.

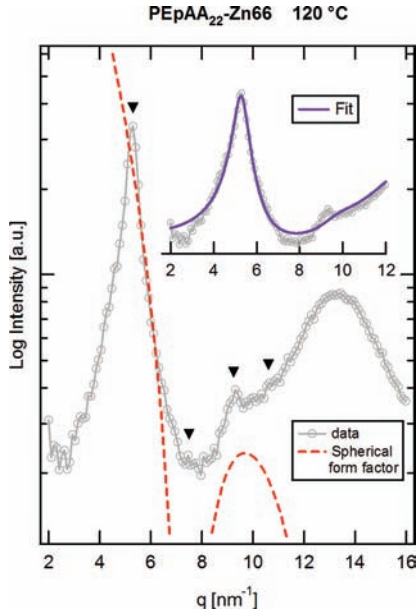

Figure 8. Scattering intensity versus q for $PEpAA_{22}$−Zn66 at 120 °C. Solid line is multifunction model (eq 1) with $R_1 = 0.54$ nm, $R_{CA} = 0.67$ nm, and $N_p = 0.42$ nm^{-3}. Dashed line is the spherical form factor for a sphere with radius 0.52 nm. Triangles are positioned at (1, $\sqrt{2}$, $\sqrt{3}$, 2)q^* which correspond to expected positions of the first four reflections for either simple cubic or body-centered cubic packing. Note that the second reflection is absent in the experimental data due to minimum in the form factor.

$PEpAA_{9.5}$−Zn116 as it is contains an excess of zinc. Fits to the KT model are not included for random ionomers $BPErMAA_4$−Zn and $PErAA_{13}$−Zn18 because at high temperature the ionomer peak is too weak and broad to be fit with confidence for these samples. At room temperature $BPErMAA_4$−Zn patterns can be fit; however, due to the breadth of the peak it is difficult to have much confidence in the parameters obtained (see Supporting Information Figure S4).

It is worthwhile to inspect the scattering from $PEpAA_{22}$−Zn66 at 120 °C more closely as shown in Figure 8. While the highly overlapped STEM images for this material suggest the aggregates may have liquidlike order, the scattering peak at $q^* = 5.3$ nm^{-1} is very sharp. There is also a second sharp peak at $q = 9.3$ nm^{-1} and an extremely weak peak at $q = 10.6$ nm^{-1}. The best fit obtained for the KT model ($R_1 = 0.54$ nm, $R_{CA} = 0.67$ nm, and $N_p = 0.42$ nm^{-3}) is shown in the inset. While the KT fit captures the first peak, it is unable to accurately reproduce the position and sharpness of the second peak. *The sharpness and position of the peaks suggest that the aggregates are arranged on a crystalline lattice rather than dispersed with liquidlike order.*

For spheres with either simple cubic (SC) or body-centered cubic (BCC) ordering, the ratio of peak positions of the first four reflections are 1:$\sqrt{2}$:$\sqrt{3}$:2, as indicated by the triangles in Figure 8. Also included in this figure is the form factor scattering for a sphere with radius 0.52 nm, which is consistent with values of R_1 obtained from the KT model. The minimum in the form factor coincides with $\sqrt{2}q^*$ which explains why this reflection is not observed in the experimental data. *Self-assembly of ionic aggregates on a lattice has never been reported for polyethylene-based ionomers.* To our knowledge, ionic aggregate ordering for ionomers with acid groups distributed along the chain has only been reported by Visser and Cooper.[3,4] They observed higher-order reflections consistent with either SC or BCC aggregate ordering for one sodium-neutralized sulfonated polyurethane ionomer with fairly well-controlled acid group spacing and the added segregation driving force of the hard segment. Precisely defining the spacing between functional groups along a linear polymer can result in ionomers with a periodic aggregate distribution. By comparing the three precise ionomers with ~75% neutralization at 120 °C (Figure 3b), the cubic order is found at the highest acid content (22 mol %). This observation is qualitatively consistent with the self-assembly of block copolymers, wherein a transition from disordered to ordered spherical micelles is expected with an increase in the minority composition. It should be noted that the cubic order remains after cooling the sample from 120 °C to room temperature. While the peaks for the pressed room temperature sample (Figure 3a) are broader than the high-temperature sample, they are not inconsistent with a cubic structure. This indicates that the sample's thermal history can influence the degree of ionic aggregate ordering observed below the melting temperature.

Differentiating between SC and BCC lattices from X-ray scattering requires seven peaks, and here the higher-order reflections are masked by the amorphous halo for PEpAA$_{22}$−Zn66. However, R_{CA} and N_p can be calculated from the first peak position and the geometry of the lattice. For SC and BCC, this yields R_{CA} = 0.59 and 0.73 nm and N_p = 0.60 and 0.42 nm^{-3}, respectively. If the aggregates adopt a SC structure, the thickness of the hydrocarbon shell around the aggregate core, $R_{CA} - R_1$, would be only 0.07 nm, whereas for a BCC structure it is a more reasonable 0.21 nm (R_1 determined by form factor scattering, Figure 8). Additionally, the values of R_{CA} and N_p for a BCC lattice are very similar to those obtained from the best KT model fit which captures the shape of the first peak well (Figure 8). For these reasons, we believe that the BCC structure is more likely, and we will use the morphological parameters corresponding to a BCC structure in the following discussion.

The composition of ionic aggregates has implications for ion mobility and transport in ionomers and remains a matter of controversy.[1] The widely used "mulitplet" model assumes that the ionic aggregates contain only ionic groups.[41] Vanhoorne and Register[40] found that the zero shear viscosity of BPErMAA$_4$−Zn54 ionomers was unaffected when 46% of the unneutralized acid groups were converted to ethyl esters suggesting the free acid groups do not effectively plasticize the ionic aggregates in zinc neutralized materials. One X-ray absorption spectroscopy study found that the local environment around zinc cations is unaffected by esterization which is interpreted as further evidence that free acid groups do not complex with the ionic aggregates.[42] If the "multiplet" model is correct, the number density of aggregates should increase linearly with the extent of neutralization at fixed acid content and the acid content at fixed neutralization level.

Figures 9 illustrates how the core radius, radius of closest approach, and number density of aggregates vary as a function of acid content for PEpAA−Zn ionomers. Clearly, changing the acid content (9.5−22 mol % acid) at fixed neutralization level (∼75% Zn) has a large effect on the morphological parameters. In contrast, increasing the neutralization level at a fixed acid content has only a modest effect. The morphological parameters for PEpAA$_{9.5}$−Zn56 and PEpAA$_{9.5}$−Zn86 are R_1 = 0.52 and 0.51 nm, R_{CA} = 1.06 and 1.03 nm, and N_p = 0.08 and 0.09 nm^{-3}, respectively. The radius of the scattering core is insensitive to acid content and neutralization level at these ranges, and the value of ∼0.5 nm obtained from the KT model and form factor estimate is in excellent agreement with several previous X-ray studies[14,15,17] of BPErMAA−Zn ionomers. This suggests that the aggregate core size may be determined by steric considerations from the chain backbone; investigating precise ionomers with varying spacer length between the acid group and the backbone would help to elucidate the factors determining the core size.

From Figure 9, it is clear that both the radius of closest approach and the number density of aggregates vary strongly with acid content at ∼75% neutralization. The morphological parameters for PErAA$_{13}$−Zn81 are R_1 = 0.43 nm, R_{CA} = 0.59 nm, and N_p = 0.18 nm^{-3}. While N_p is nearly identical for PErAA$_{13}$−Zn81 and PEpAA$_{13}$−Zn82 (0.18 and 0.17 nm^{-3}, respectively), R_{CA} is significantly smaller for the former (0.59 nm versus 0.88 nm), suggesting that the number of aggregates

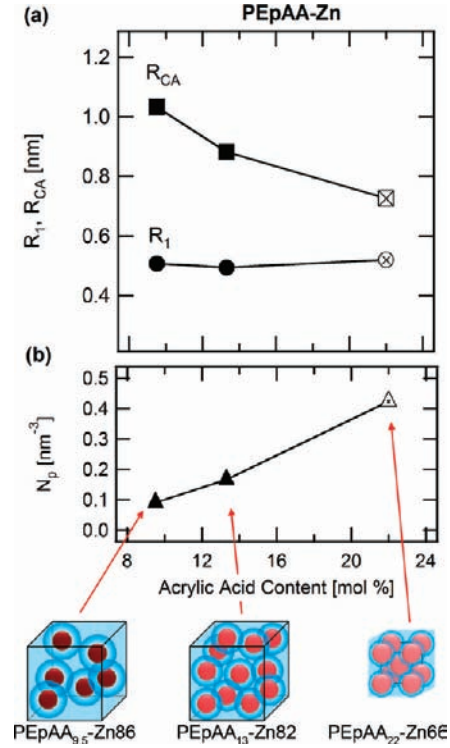

Figure 9. Morphological parameters obtained from the scattering data at 120 °C for PEpAA−Zn ionomers with ∼75% neutralization. Solid symbols were obtained from fits to the KT model, and open symbols were derived by assuming BCC packing of ionic aggregates with R_1 estimated from form factor contribution (see Figure 8). Solid lines are guides to the eye only. Note the increase in N_p with increasing acid content is more rapid than predicted by a fixed aggregate composition. Three-dimensional schematics of the morphology of PEpAA$_{9.5}$−Zn86 (left), PEpAA$_{13}$−Zn82 (center), and a BCC unit cell of PEpAA$_{22}$−Zn66 (right) are based on the parameters in the graphs. The radius of closest approach is shown in blue, while the aggregate core is shown in red. The relative ionic content of the aggregate, assuming all the acid groups associate with the aggregate, is depicted by the intensity of the core color with lighter shades indicating less ionic content.

is controlled by the acid content and neutralization level but the separation between aggregates is determined by the acid distribution. The radius of closest approach for precise ionomers decreases from ∼1.1 to 0.72 nm as the acid content increases from 9.5 to 22 mol % (**9a**). This indicates that the closest approach of the aggregates is dominated by the length of the PE sequence between acid groups. Consistently, the number density of aggregates increases dramatically with increasing acid content. As the acid content is increased from 9.5 to 22 mol % at constant neutralization level (∼75% Zn), the number density of aggregates increases by a factor of ∼5. This is double the factor of 2.3 expected for a fixed aggregate size and composition. *Therefore, as acid content increases, the aggregates become less ionic, more numerous, and closer together until at the highest acid content they self-assemble onto a cubic lattice.*

Comparing the published scattering pattern[14] for BPErMAA$_{13}$−Zn60 with BPErMAA$_4$−Zn55 in Figure 3b shows that both ionomers have broad peaks centered around $q \approx 3$ nm^{-1}. This indicates that the position of the ionomer peak is insensitive to acid content for branched, random polyethylene ionomers. An insensitivity of ionomer peak position to acid content has also been observed in random poly(styrene-*ran*-methacrylic acid)−Cu ionomers.[43] The highly variable acid spacing in the random ionomers leads to a large polydispersity

(41) Eisenberg, A.; Hird, B.; Moore, R. B. *Macromolecules* **1990**, *23*, 4098.
(42) Grady, B. P.; Floyd, J. A.; Genetti, W. B.; Vanhoorne, P.; Register, R. A. *Polymer* **1999**, *40*, 283.

in correlation length between aggregates and thus to a very broad scattering feature which may mask the effect of acid content on the number density of aggregates. In contrast, the stronger and more well-defined ionomer peak for precise ionomers shifts from $q \approx 3.1$ to 5.3 nm^{-1} as the acid content increases from 9.5 to 22% at a neutralization level of ~75% Zn (Figure 3b). Thus, by reducing the polydispersity in correlation lengths between ionic aggregates by precisely controlling acid placement, the changes in ionomer morphology can be more confidently identified and quantified.

Since the scattering data suggest that the variation in the number density of aggregates is inconsistent with aggregates of fixed size (as evidenced by the KT model) and fixed composition (as posited by the multiplet model), the alternative extreme is to assume that all the acid groups, whether neutralized or not, are incorporated into the aggregate core. Following the analysis presented in references 20 and 26, the ~0.5 nm aggregates can accommodate more acid−ion pairs than are available; therefore, it is assumed that all unneutralized acid groups are associated with the ionic aggregates. This assumption is partly justified by the enthalpic penalty for incorporation of the unneutralized acid groups in the nonpolar PE matrix. In this case, the aggregates would become more ionic as the neutralization level is increased, but less ionic as the acid content increases to be consistent with the substantial increase in N_p with acid content. The 3D schematics in Figure 9 illustrate the differences in morphology for PEpAA−Zn ionomers as well as how the relative ionic content of the aggregates would change if all the acid groups were associated with the aggregates. As the acid content increases, the ionic aggregate size is constant while they become more numerous (N_p increases), closer together (R_{CA} decreases), and less ionic. While the relative ionic content of the aggregates would change if some of the unneutralized acid groups reside in the matrix (this would affect the relative shading of the aggregates in Figure 9), the size, closest approach, and number density of aggregates represented in the schematic would remain as drawn.

Conclusions

This work investigated the effect of acid placement, acid content, and neutralization level on the morphology of linear poly(ethylene-*co*-acrylic acid)−Zn ionomers. For the first time, the effect of random and precise acid placement on ionomer morphology has been isolated, and cubic ordering of ionic aggregates in polyethylene-based ionomers has been observed. The main conclusions are as follows:

- HAADF-STEM confirms that the ionic aggregates are roughly spherical.
- Precise ionomers with an acid group on every 21st carbon ($PEpAA_{9.5}$−Zn) are semicrystalline at room temperature and interpretation of their scattering room temperature X-ray is complicated by the convolution of scattering contributions from both layers of acid dimers associated with crystallites and interaggregate scattering from ionic aggregates in the amorphous regions. Partial deconvolution of the relative contributions can be achieved via drawing samples.
- Scattering features associated with the ionic aggregates arise from interaggregate interference, and the KT model does an excellent job describing the scattering from precise ionomers with 9.5 and 13 mol % acid. The reduced polydispersity in correlation lengths in precise ionomers gives rise to much more intense and well-defined peaks and therefore greater confidence in structural information determined from the KT model parameters.
- For the partially neutralized precise ionomer with the highest acid content ($PEpAA_{22}$−Zn66) at 120 °C, the ionic aggregates self-assemble onto a cubic lattice.
- The aggregate core size is ~0.5 nm by X-ray scattering and is independent of acid content and neutralization level. The radius of closest approach and number density of aggregates are strongly affected by acid content. As the acid content is increased from 9.5 to 22 mol % at a fixed neutralization level (~75% Zn), the number density of aggregates increases by a factor of ~5. The variation in the number density of aggregates as a function of acid content is inconsistent with the multiplet model assumption that the aggregates have a fixed composition.

This study of precise ionomers lends considerable new insights into ionomer morphology. These model materials will remain valuable for continuing efforts to determine the exact composition of the ionic aggregates and the extent to which unneutralized acid groups associate with the aggregates. Multiscale modeling of these precise ionomers that incorporates ionic associations as well as polymer conformation may be able to shed light on the factors determining the ionic aggregate radius and radius of closest approach as well as the aggregate composition. Additionally, spectroscopic studies using these precise materials could address ionic aggregate composition and local structure due to their greatly reduced variability compared to the random ionomers studied to date. Lastly, the implications of regularly ordered aggregates for mechanical and transport properties of ionomers remain to be explored.

Acknowledgment. We thank Wenqin Wang (UPenn) for insightful discussions. This work was supported by the National Science Foundation Polymers Program, Grant DMR 0549116 (Winey) and Florida Space Grant Consortium (NASA-FSGC).

Supporting Information Available: Experimental details and supplemental figures: room temperature scattering curves for $PEpAA_{13}$−Zn82 and $PErAA_{13}$−Zn81 (Figure S1), scattering for $PEpAA_{9.5}$−Zn0 as a function of temperature (Figure S2), comparison of scattering at room temperature and 120 °C for $PEpAA_{9.5}$−Zn ionomers (Figure S3), and scattering curves over an expanded q range for $BPErMAA_4$−Zn78 at room temperature and 120 °C (Figure S4). This material is available free of charge via the Internet at http://pubs.acs.org.

JA101991D

(43) Wang, W.; Chan, T.-T.; Perkowski, A. J.; Schlick, S.; Winey, K. I. *Polymer* **2009**, *50*, 1281.